Aerodynamic Characteristics of Dimple Effect on Airfoil

Elhassen A. A. Omer[1] , Hana M. Momen[2] and Rayan N. Yahia[2]

[1]Zawia University, Faculty of Engineering, Mechanical Engineering Department.
E. mail : e.amr@zu.edu.ly
[2]Tripoli University, Faculty of Engineering, Aeronautical Engineering Department.

Abstract

The present work describes aerodynamics enhancement of flow over an airfoil by applying certain surface modifications in form of dimples. This was done on the symmetric four digit NACA 0012 airfoil. The dimples were implemented on the upper surface of a two dimensional airfoil model, and placed at 25%, 50% and 75% of the chord length and simultaneously compared with the smooth airfoil. A comparative study of surface modified airfoil models to investigate lift and drag for a constant Re at various angle of attacks (AOA). The two dimensional airfoil was analyzed with and without dimples using a CFD Code ANSYS Fluent 2022R1 software. From this investigation it has been observed that the flow separation on the airfoil can be delayed by using dimples on the upper surface, it was found that the dimples located at 0..75c has the best aerodynamic enhancement where the lift and drag coefficients improved by 17% and 6% than the smooth airfoil respectively. Also, stall AOA increased by two degrees. Also, the analysis favours the dimple effect by increasing L/D ratio and thereby providing the maximum aerodynamic efficiency, which provides the enanced performance of airfoils.

Keywords : Airfoil, Lift, Drag, Surface modification, dimples, aerodynamic performance.

Introduction

Airfoil is a two dimensional cross section of a wing. Hence the aerodynamic properties of the airfoils directly affect the aerodynamics of the wing. The surface modifications are vital in improving the aerodynamic performance of an airfoil and they are really effective in altering the boundary layer by creating vortices which delays the boundary layer separation resulting in decrease of pressure drag and also increase in the angle of stall. The dimples are widely considered as one of the techniques to modify the surface of an airfoil. Kumar et al. [1], Amit et al. [2] and Bogdanovic-Jovanovic et al. [3] found that dimples are critical in airfoil to reduce the drag. They also observed that introduction of dimples produce turbulence that delays the separation of the boundary layer and decreases the formation of the wake. The experimental results of the distribution of surface pressure indicate that flow separation occurs and the boundary layer is delayed by dimples. Separation by producing more turbulence over the

surface, thereby reducing the development of wake, demonstrates that the dimple change the stall angle.

Wang et al. [4] studied the aerodynamic performance of the S809 airfoil with and without surface modifications using CFD simulations. The results showed that it can effectively improve the aerodynamic performance of the S809 airfoil, reduce the thickness of the boundary layer, and delay stall. The double-row arrangement demonstrated a good performance in controlling flow separation, which further improved the aerodynamic performance of the S809 airfoil. Devi et al., [5] analyzed triangular and square cavity on symmetric NACA 0012 airfoil. Square cavity improved lift coefficient by 29.05%. Saraf et al., [6] analysed NACA0012 airfoil by varying the location of outer dimples and concluded that dimples at 75% of the chord length has a 7% increase in lift coefficient. Rajasai et al., [7] analysed the effects of circular dimples on NACA 2412 airfoil and concluded that the presence of a dimple increases the stall angle of the aircraft. Mustak and Harun, [8], showed that at zero degree angle of attack, dimples on airfoil do not shows changes in drag compared to smooth airfoil. But at high angles of attack it behaves like bluff body. It leads to delay in separation and wake formation. Also it increases the angle of stall.

In this paper, a symmetrical airfoil NACA 0012 is modified with semi-circular dimples made on the upper surface of the airfoil. This airfoil was chosen because it has been used in many constructions. Typical examples of such use of the airfoil are the B-17 Flying Fortress and Cessna 152, the helicopter Sikorsky S-61 SH-3 Sea King as well as horizontal and vertical axis wind turbines, [9]. Through this study we aim at making aircrafts more maneuverable by dimpled airfoils. Also we are looking to improving performance by more L/D ratio i.e. increasing aerodynamic efficiency. The current study focuses on studying the effects of surface modification over NACA0012 airfoil on aerodynamic performance through CFD analysis.

Mathematical Modelling

In CFD, RANS is the most widely used turbulence modelling approach. In this approach, the model is governed by the incompressible, steady 2-dimensional form of the continuity and averaged Navier–Stokes equations, [10, 11]. In the Cartesian tensor system these equations can be written as :

$$\frac{\partial}{\partial x_i}\ (\rho u_i) = 0 \tag{1}$$

$$\frac{\partial}{\partial x_j}\left(\rho u_j u_i\right) = -\frac{\partial P}{\partial x_i} + \frac{\partial}{\partial x_j}\left[\mu\left(\frac{\partial u_i}{\partial x_j} + \frac{\partial u_j}{\partial x_i}\right)\right] + \frac{\partial}{\partial x_j}\left(-\rho\overline{u_i' u_j'}\right) \tag{2}$$

The normal Reynolds stress which is combined by Boussinesq relationship and the eddy viscosity is given by

$$-\rho\overline{u_i' u_j'} = \mu_t\left(\frac{\partial u_i}{\partial x_j} + \frac{\partial u_j}{\partial x_i}\right) \tag{3}$$

The k-omega SST turbulence model includes transport of the turbulence shear stress in the definition of the turbulent viscosity. These features make this model more accurate and reliable for a more comprehensive class of flows (for example, adverse pressure gradient flows, airfoils, and transonic shock waves) than the standard model. k-ω model, [12].

The k-ω SST turbulence model is a combined version of the k-ε and the k-ω turbulence models [13], and is governed by:

$$\frac{\partial}{\partial x_i}(\rho k u_i) = \frac{\partial}{\partial x_j}\left[\left(\mu + \frac{\mu_t}{\sigma_k}\right)\frac{\partial k}{\partial x_j}\right] + G_k - Y_k + S_k \quad (4)$$

$$\frac{\partial}{\partial x_i}(\rho \omega u_i) = \frac{\partial}{\partial x_j}\left[\left(\mu + \frac{\mu_t}{\sigma_\omega}\right)\frac{\partial \omega}{\partial x_j}\right] + G_\omega - Y_\omega + D_\omega + S_\omega \quad (5)$$

Where : σ_k represents the generation of turbulence kinetic energy due to mean velocity gradients. σ_ω represents the generation of ω. Y_k and Y_ω represent the dissipation of k and ω due to turbulence. D_ω represents the cross-diffusion term. S_k and S_ω are user-defined source terms.

The term Gk represents the production of turbulence kinetic energy due to mean velocity gradient that can be calculated by

$$G_k = -\rho\overline{u_i' u_j'}\frac{\partial u_j}{\partial x_i} \quad (6)$$

The production of ω is given by equation

$$G_\omega = \beta\frac{\omega}{k}\ G_k \quad (7)$$

The coefficient β is a function of k and ω and it is so calculated that in the far field regions of flow approaches to unity.

Computation Domain

The geometry of smooth airfoil NACA0012 was prepared by coordinates taken from [14] and plotted as shown in Fig. (1a). The C-shaped domain was considered around the airfoil with given dimensions to obtain a domain-independent solution.as shown in Fig. (1b).

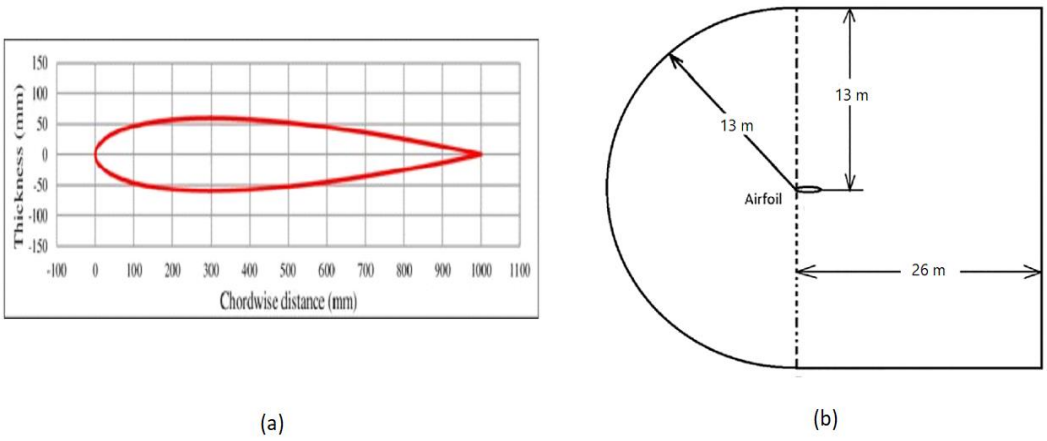

(a) (b)

Fig. 1: (a) The NACA 0023 airfoil, (b) The computational domain dimensions

Fig. (2) shows a schematic diagram of the 2D computational domain with named boundaries. On the vertical edge of the computational domain pressure outlet boundary condition was assumed and the velocity inlet boundary condition on the remaining outer edges of the computational domain. The airfoil surfaces are treated as no-slip walls with zero velocity was ensured on the airfoil surfaces.

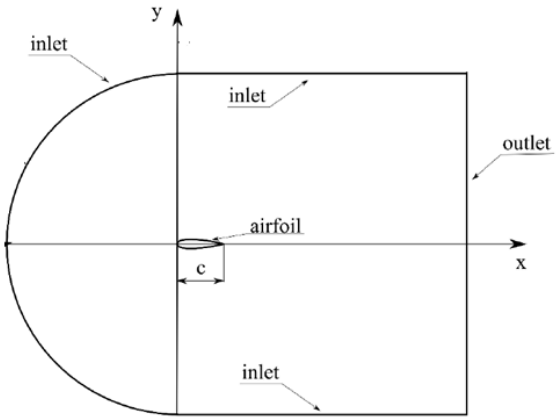

Fig. 2: The named boundaries of the computational domain

Airfoil Characteristics Analysis

In order to compare aerodynamic characteristics of different airfoil geometries, it is common to analyze the variation of their aerodynamic coefficients with the angle of attack (AoA). Thus, the lift and drag for a fixed shape and at a fixed angle of attack. Then can be defined as, [15] :

$$C_L = \frac{F_L}{\frac{1}{2}\rho u_\infty^2 \, c} \tag{8}$$

$$C_D = \frac{F_D}{\frac{1}{2}\rho u_\infty^2 \, c} \tag{9}$$

Also, it is common to plot the lift coefficient as a function of the drag coefficient, often called drag polar, which provides an overview of aerodynamic performance of flow over airfoils. Aerodynamic efficiency is defined as the ratio of lift coefficient over drag coefficient

$$E = \frac{C_L}{C_D} \tag{10}$$

Hence, the aerodynamic efficiency can be improved by either increasing the lift coefficient or decreasing the drag coefficient.

Solution Methodology

The modeling of the airfoils was done using the Design Modeler component of the ANSYS software. The airfoil was plotted by importing the data points then the surface modification was designed on it. The chord length of the airfoil was set to one meter. The upper surface of the airfoil was modified by creating dimples of a diameter of 0.03% of chord length, and at different chordwise locations namely, 25%, 50% and 75% of chord.

Meshing of the domain was done using unstructured mesh with tetrahedral elements. The resolution and density of the mesh is greater in regions where superior computational accuracy is needed, such as the near wall region of the airfoil. Body of influence was created around the airfoil to give finer mesh with element size of 0.02m as shown in Fig. (3a). Inflation was used over the surface of airfoil with 25 layers with first layer with cell width of 0.01mm with cell growth ratio of 1.1 as the shown meshing at the airfoil dimpled surface in Fig. (3b).

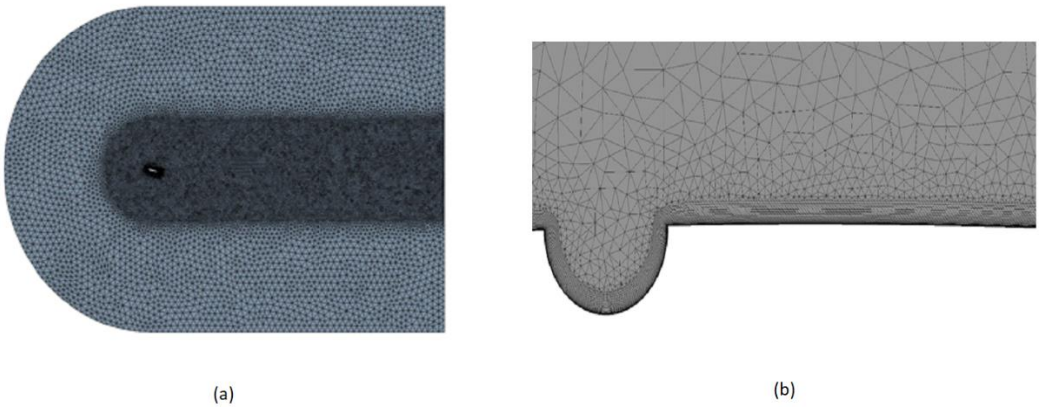

Fig. 3: (a) Mesh of the computational domain around NACA 0012 airfoil, (b) closed detail to the dimpled airfoil surface.

For precise simulation of the boundary-layer flows and the coupled lift and drag forces of airfoils, the average value of y^+ which is a non-dimensional distance from the wall to the first node of the mesh was kept under one ($y^+<1$) for resolving the boundary layer on the mesh.

The incompressible, two-dimensional steady Reynolds averaged Navier–Stokes (RANS) equations were employed and discretized using the finite volume method. To solve the coupled problem between pressure in momentum equations and velocity components, semi-implicit method for pressure-linked equations (SIMPLE) algorithm was employed, and second-order upwind spatial discretization was set in calculation. The spatial gradient was selected as the least squares cell based. The flow around the NACA 0012 airfoil was numerically investigated using the commercial Computational Fluid Dynamics (CFD) code ANSYS22 R1. To investigate the aerodynamic characteristics of the NACA 0012 airfoil, the k-ω SST turbulence model was adopted.

The turbulence intensity and length scale were used to specify (k) and (ω) at the inlet, where I is taken as 0.05 and l = 0.01m. Velocity at inlet was specified to achieve the desired Re. Air pressure was taken as standard. In monitors section, Convergence criteria are set such that the normalized residuals for each parameter are less than 10E-6 for higher accuracy.

Standard initialization was used with declared inlet conditions to initialize the solution. Calculation was carried out for more 2000 iterations or until all scaled residuals was achieved or constant Cl and Cd residuals were achieved. Fig. (4) gives an example of the convergence history for the scaled residuals, and lift coefficient.

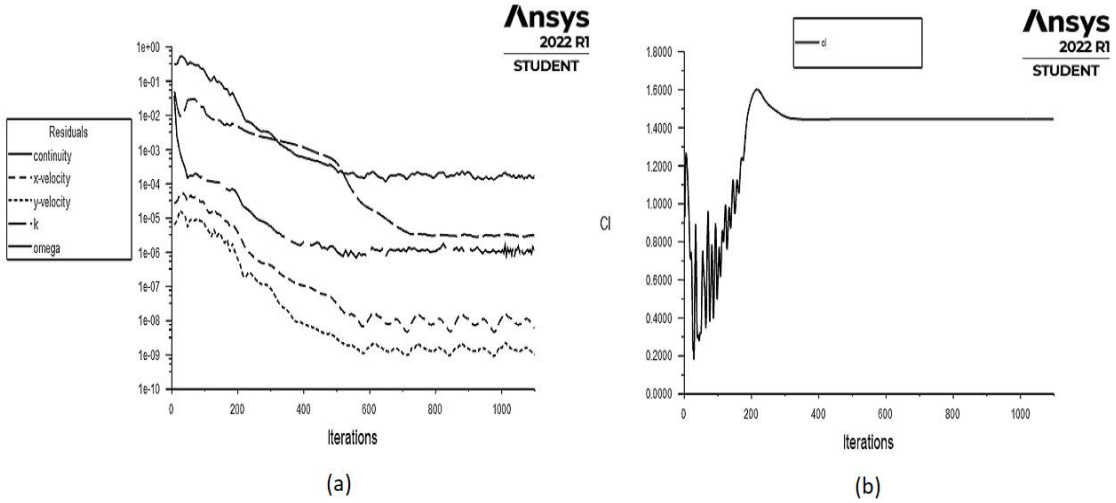

Fig. 4: Example of the convergence history for (a) the scaled residuals and (b) lift coefficien

Mesh Sensitivity and Code Validation

A grid independence study was conducted to select an optimum mesh number which guarantees that the solution is independent of the mesh resolution. The mesh independence testing is performed and the mesh refinement is assessed by means of the lift and drag coefficients variations. For that purpose, five different meshes were used, the Reynolds number and angle of attack were kept constant at 3.0E +6 and $\alpha = 15^{o}$ respectively. Fig.(5a) shows the results of the test for each mesh. It is noticed that there is no significant difference in the computed results between the fourth and fifth grids. Hence, by a compromise between required accuracy and computation time, the fourth grid is selected for the simulations.

The present study results were compared to these obtained by experimental and numerical work of Eleni, et al, [9]. The results were obtained for a Re = 3.0E +6 . The lift coefficients variations with the angle of attack are shown in Fig. (5b). It is clear that a good agreement is reached between the numerical results and the experimental and numerical data in the literature

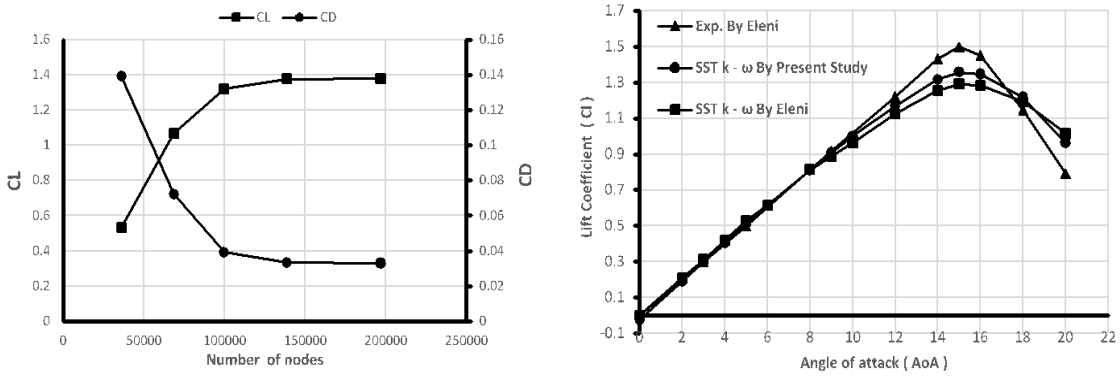

(a) (b)

Fig. 5: (a) Grid independence testing (b) Present study comparison with Eleni [9] results.

Results and Discussion

The results of lift and drag coefficients of dimpled airfoils with respect to the smooth airfoil are plotted as shown in Fig (6) . All dimpled airfoils did not provide better result at low angles of attack, ($0° \leq \alpha \leq 10°$). For higher angles of attack, the near stall region there is an improvement of aerodynamic performance for all dimpled airfoils, where it can seen an increase in lift coefficient and reduction in drag coefficient. From Fig. (6a), it can be found that using the semi-circular dimple at all locations significantly higher than that of smooth airfoil after 10 degree angle of attack.

The dimple at a location 075c has the highest lift coefficient at the stall angle with an increase of 11% than the smooth airfoil. It can also be noted that the stall angle increased by 2 degrees. After the stall angle, the lift coefficient starts to decrease as the angle of attack increases. From Fig. (6b), for drag coefficients, it can be found that the airfoils with dimple has no effect at low AoA less than 12^o, as AoA increases the modified airfoils gave a reduction of drag. after reaching the stall angle, the drag coefficient were sharply increasing. The one with dimple at 75% of chord length does decrease the drag by around 1.0 - 3 % at higher angles of attack. The performance of any airfoil is measured by aerodynamic efficiency curve which shows the combined effect of lift and drag ratio as shown in Fig. (7). Generally, all four models show an increase in the L/D ratio till they attain a maximum value and thereafter it decreases. For low attack angles ($0° \leq \alpha \leq 4°$), the airfoil surface modification has no effect and all airfoils have a similar aerodynamic efficiency curve. At higher angles of attack ($5° \leq \alpha \leq 20°$), all modified models show higher aerodynamic efficiency than smooth airfoil. It can be seen, the optimum AoA is obtained at 8^o for smooth airfoil.

.

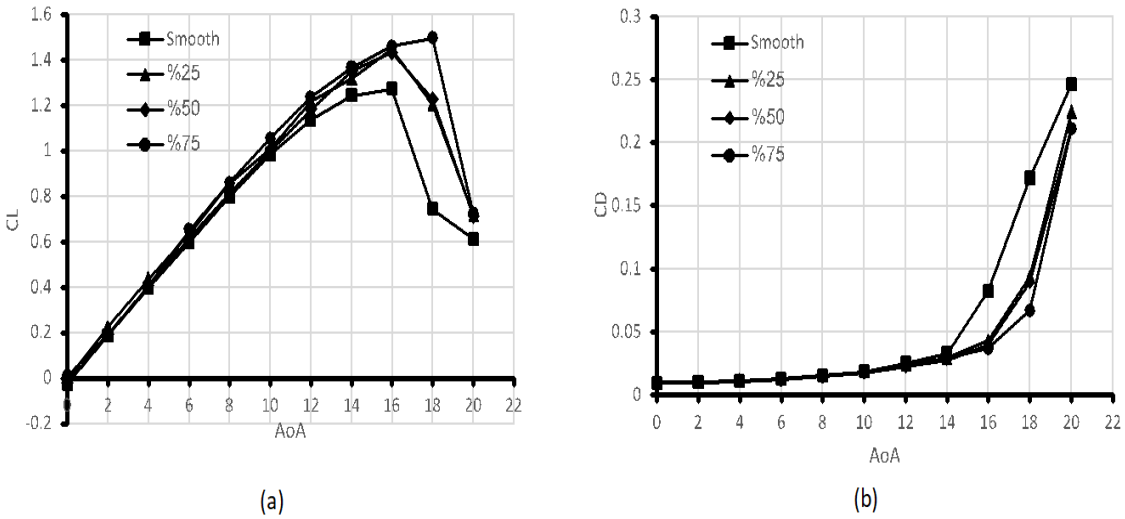

Fig. 6: Comparison of dimpled and smooth airfoils. (a) Lift coefficients and (b) Drag coefficients

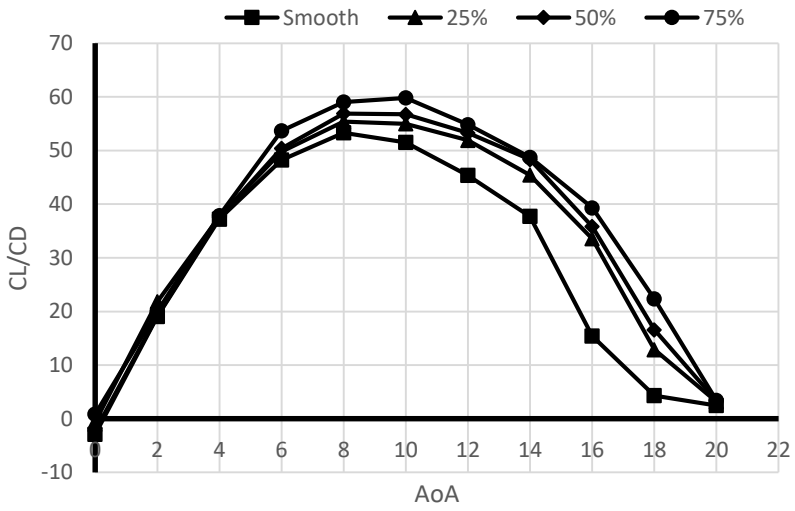

Fig. 7: Aerodynamic efficiency comparison of dimpled and smooth airfoils.

Using a single dimple the optimum AoA increased to 10º for the dimpled airfoils, the reason is that the C_L produced is much more significant than C_D. Also, it can be seen that the dimpled airfoil with dimple at 0.75c location has the highest efficiency and best performance

Fig. (8) and Fig, (9) show the static pressure and velocity magnitude contours respectively. These contours are for smooth and 0.75c dimpled airfoils at various angles of attack were compared. Generally, it is seen that the upper surface of the airfoils is at low pressure and high velocity, and the lower surfaces are at high pressure and low velocity. This is due to the characteristic structure of airfoils. As a result, the incoming airflow effectively pushes the airfoil upwards, and the lift generated.

Fig. (8) shows that at zero degree angle of attack, upper side and lower side pressure is approximately equal so their lift is minimum. As the angle of attack increased, results show that pressure on upper side started decreasing and on lower side it started increasing. It is very evident that at higher AOA the flow tends to separate from trailing edge. The presence of dimple imparts the turbulent kinetic energy which helps in reattached of flow and hence flow adheres to the airfoil surface. Therefore at higher angles off attack, the lift generated by dimpled airfoil is higher associated with reduction in drag.

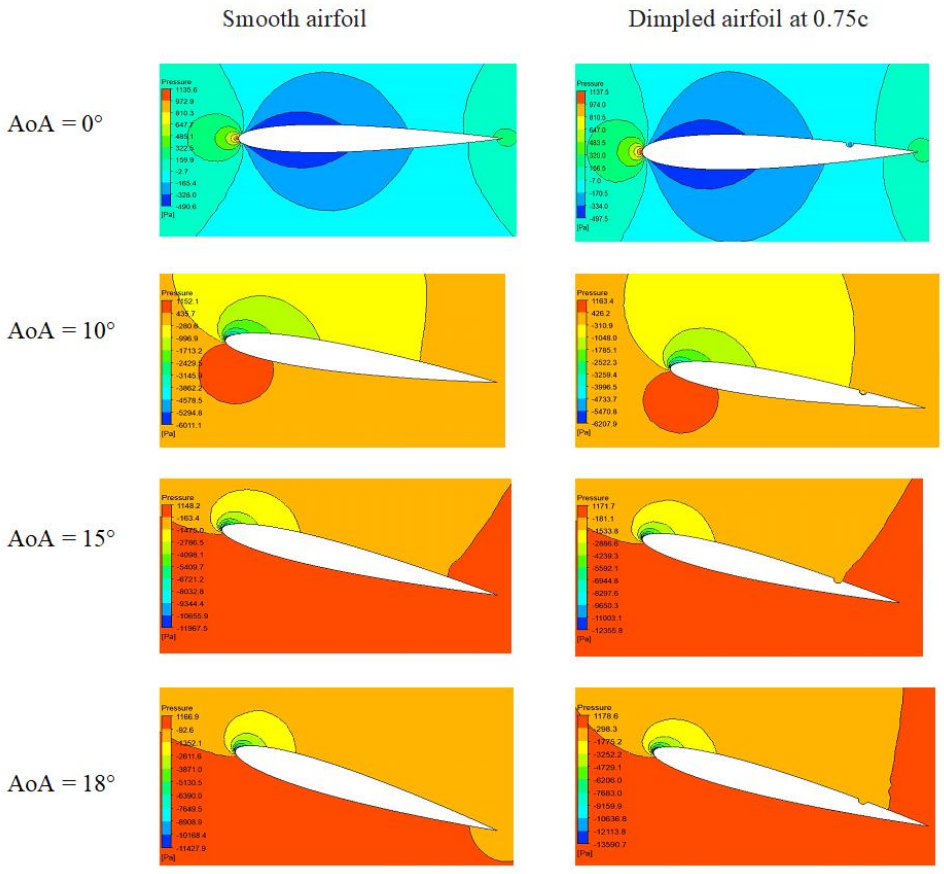

Fig. 8: Pressure contours for smooth and dimpled airfoils.

Fig. (9) shows that velocity on upper and lower side of the airfoil is approximately similar at zero degree angle of attack. Flow over the airfoil boundaries is intact from the angle of 0^{o} to

10^o, there is no flow separation and the lift curves are aligned for both smooth and dimpled airfoils. At 10^o angle of attack fluid starts separating and generates wakes. This leads to pressure drag. Contours of velocity at a 15^0 angle of attack for the smooth and dimpled airfoils are compared. Flow separation is delayed for the airfoils with dimples. Hence, dimples produce stream-wise vortices that carried higher momentum flow in the boundary layer, which kept the flow attached to the surface of the airfoil and, in turn, delayed separation, and thus enables a higher lift coefficient during and lower drag. As AoA reaches 18^o angle of attack separation reaches maximum value, after that lift starts decreasing.

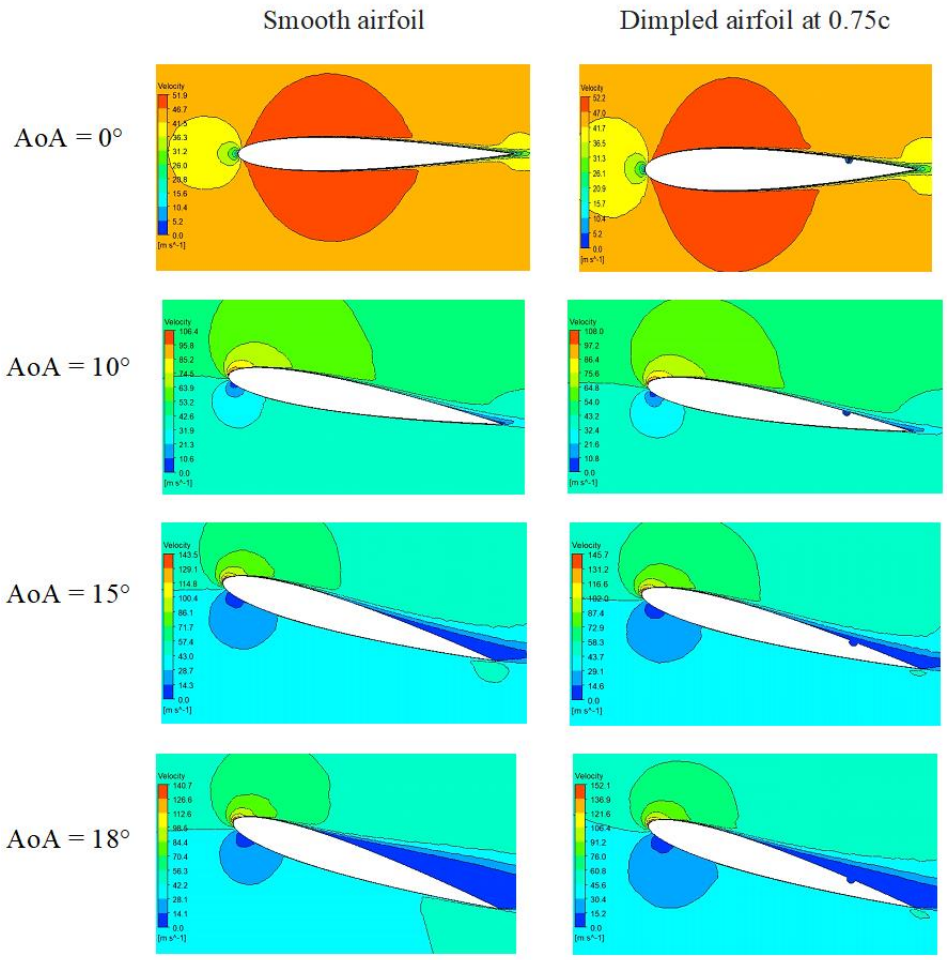

Fig. 9: Velocity contours for smooth and dimpled airfoils.

CONCLUSIONS

A CFD simulation study of the aerodynamic performance of surface modified NACA0012 airfoils are presented and compared with smooth airfoil. The simulations performed by ANSYS

Fluent 2022 R1. The flow was considered fully turbulent and SST k-ω turbulence model is used. The study for constant inlet velocity (i.e. constant Re = 3E+6) and the range of the AoA of this simulation was between 0^o to 20^o. From the results, the following important issues were conclude :

1. The modified surface airfoils showed an enhancement of aerodynamic performances compared to smooth airfoil.
2. The location of the dimple on the airfoil plays an important role. Airfoil with dimple at 75% of the chord length was the most suitable location for better aerodynamic performance.
3. The airfoil with dimple at 75% of chord length also increases the maximum lift coefficient of the airfoil by 11%, while coefficient of drag has been reduced by 3%.
4. The airfoil with dimple at location 75% of chord length successfully controls the boundary layer separation causing an increase of stall angle by 2 degrees.
5. The aerodynamic efficiency was improved where the optimum AoA increased to 10^o for the dimpled airfoils, instead of 8^o for smooth airfoil.

Nomenclature

c	Chord length, m.	***Greek symbols***	
C_D	Drag coefficient.	ε	Dissipated turbulent kinetic energy, m^2/s^3.
C_L	Lift coefficient.	α	Angle of attack
E	Aerodynamic efficiency.	μ	Dynamic viscosity, kg/ms.
F_D	Drag force, N/m.	ρ	Density, kg/m^3
F_L	Lift force, N/m.	ν	Kinematic viscosity, m^2/s.
I	Turbulence intensity.	μ_t	Eddy viscosity, kg/ms.
i,j	Indices.	ω	Specific turbulence dissipation rate, m^2/s.
l	Turbulent scale length, m.	***Abbreviations***	
k	Turbulent kinetic energy, m/s^2.	AoA	Angle of attack
P	Pressure, Pa.	CFD	Computational Fluid Dynamics
P_∞	Free stream pressure, Pa.	FVM	Finite Volume Method
Re	Reynolds number.	NACA	National Advisory Committee for Aeronautics
u	Velocity component, m/s.		
u_∞	Free stream velocity, m/s.	RANS	Reynolds-Averaged Navier Stokes
x	Coordinate / axial distance, m.	SST	Shear Stress Transport
y^+	The normalized thickness of first layer surface.	grids perpendicular to the airfoil	

REFERENCES

[1] Kumar, S. N., Hari A. V., and Pillai, A. K., "Numerical Studies to Improve the Aerodynamic Efficiency of an Airfoil Using Delta-Shaped Surface Protrusions", AIP Conference Proceedings 2134, 020009, (2019).

[2] Amit, K. S., Mahendra, P., and Chouhan, T., "Review on Aerodynamic Behavior of Airfoil when Surface Modified", International Journal of Scientific & Engineering Research , pp: 516-519, (2016).

[3] Bogdanovic-Jovanovic, B. J., Zivojin M. S., and Milos M. K., "Experimental and Numerical Investigation of flow around a sphere with dimples for various flow regimes", Thermal Science, Vol.16, No.4, (2012).

[4] Wang, H.; Zhang, B.; Qiu, Q.; Xu, X. "Flow control on the NREL S809 wind turbine airfoil using vortex generators", Energy, Vol. 118, pp:1210–1221, (2017).

[5] Rajasai, B., Ravi T., and Srinath, S., "Aerodynamic effects of dimple on aircraft wings", Int. J. Adv. Mech. Aero. Engg., Vol. 2. No. 2, pp:169-172, (2015).

[6] Devi, B., and Shah, A. D., "Computational Analysis of Cavity Effect over Aircraft wing", World Engineering and Applied Sciences Journal, Vol. 8, No. 2, pp : 104 -110, (2017).

[7] Prasath. M. S., and Irish A. S., "Effect of Dimples on Aircraft Wing", GRDJE, Vol. 2, No. 5, pp: 234-242, (2017).

[8] Mustak, R., and Harun, M., "Improvement of Aerodynamic Characteristics of an Airfoil by Surface Modification", American Journal of Engineering Research (AJER), pp: 07-14, (2017).

[9] Eleni, D. C., Athanasios, T. I., and Dionissios, M. P., "Evaluation of the turbulence models for the simulation of the flow over a National Advisory Committee for Aeronautics (NACA) 0012 airfoil", Journal of Mechanical Engineering Research Vol. 4(3), pp:100 -111, (2012).

[10] Hami, K., "Turbulence Modeling a Review for Different Used Methods", International Journal of Heat and Technology, Vol. 39, No. 1, pp: 227 – 234, (2021).

[11] Lars Davidson, "Fluid mechanics, turbulent flow and turbulence modeling", Division of Fluid Dynamics, Department of Mechanics and Maritime Sciences, Chalmers University of Technology, SE-412 96 Goteborg, Sweden, (2022)

[12] Olayemi, O. A., Ogunwoye, O. V., Olabemiwo, J. T., Jinadu, A., and Odetunde, C., "Analysis of flow characterstices around an inclined NACA0012 airfoil using various turbulence models", International Conference on Engineering for Sustainable World, ICESW (2020).

[13] Menter, F. R., Review of the SST Turbulence Model Experience from an Industrial Perspective", International Journal of computational Fluid Dynamics, Vol. 23, (2009).

[14] https://confluence.cornell.edu/download/attachments/144976439/naca0012coords.txt? version=1& modification Date=1302377518000&api=v2".

[15] Anderson, J. D., "Fundamentals of Aerodynamics", McGraw Hill Series, Third Edition, (2012).

[16] ANSYS Fluent Theory Guide, Release 19.0.; ANSYS, Inc.: Canonsburg, PA, USA, (2019).